# Supporting Information

## Low-crystalline nickel hydroxide nanosheets embedded with $NiMoO_4$ nanoparticles on nickel foam for high-performance supercapacitor applications

Y.B. Chen, J.J. You, Y.H. Chen, L. A. Ma*, H.X. Chen, Z.H. Wei, X. Y. Ye*, L. Zhang*

School of Materials Science and Engineering, Fujian University of Technology, Fuzhou 350118, China

Corresponding Author

mla728@hotmail.com, creekye@163.com , leizhang@fjut.edu.cn

**Material characterization**

**Electrochemical measurements**

**Figure S1~S9**

**Table S1~S3**

## 1. Material characterization

The phase, morphology and microstructure of the synthesized samples were characterized by an X-ray diffractometer (XRD, Bruker, Germany), field emission scanning electron microscope (FESEM, NovaNano-450 FEI) and transmission electron microscope (TEM, JEM-2100). The surface characteristics of the samples were analyzed by X-ray photoelectron spectroscopy (XPS, Escalab250). The $N_2$ adsorption-desorption isotherm was determined by Brunauer-Emmett-Teller (BET) theory with the surface area analyzer (BSD 3H-2000PS1, BeiShiDe Instrument).

## 2. Electrochemical measurements

Electrochemical tests of the samples were performed using electrochemical workstation (PGSTAT302N, AUTOLAB) in a 2 M KOH electrolyte. In the three electrode test, NiMo-LDH on NF was used as the working electrode, Hg/HgO as the reference electrode, Pt plate as the counter electrode. In the ASC measurement, NiMo-LDH was used as the positive electrode and AC as the negative electrode. Cyclic voltammetry (CV) and Galvanostatic charge / discharge curves of NiMo-LDH were recorded in the potential window -0.2V to 0.8V at ranging from 10 to 100 mV and 0V to 0.5V at ranging from 4 to 12 mA cm$^{-2}$, respectively. Electrochemical impedance spectroscopy (EIS) was performed in the frequency range of 100 kHz to 0.01 Hz. The capacitance of the electrode can be calculated from the GCD curve according to equations (1) and (2):

$$C_A = \frac{I \times \Delta t}{S \times \Delta V} \qquad (1)$$

$$C = \frac{I \times \Delta t}{m \times \Delta V} \qquad (2)$$

Where $C_A$ (F $cm^{-2}$) represents the areal capacitance of NiMo-LDH, C(F $g^{-1}$) stands for specific capacitance, I (A) refers to the charge and discharge current of GCD, S ($cm^2$) is the geometrical area of NiMo-LDH , m (g) represents the mass loading of the active material, ΔV(V) represents the potential.

In ASC system, Ni2Mo1-urea 0.2M (~ 2.2 mg/$cm^2$), AC (~2.9 mg/$cm^2$) and 2 M KOH were used as positive electrode, negative electrode and electrolyte, respectively. The charge balance between the two electrodes obeys the relationship $q^+ = q^-$ and $q = C_A \times S \times \Delta V$ [S1]. Total electroactive mass of the ASC device was ∼5.1 mg.

The energy density (E, Wh $kg^{-1}$) and power density (P, W $kg^{-1}$) of the ASC devices were calculated based on GCD curves as followed:

$$E = \frac{C \times \Delta V^2}{2 \times 3.6} \qquad (3)$$

$$P = \frac{3600 \times E}{\Delta t} \qquad (4)$$

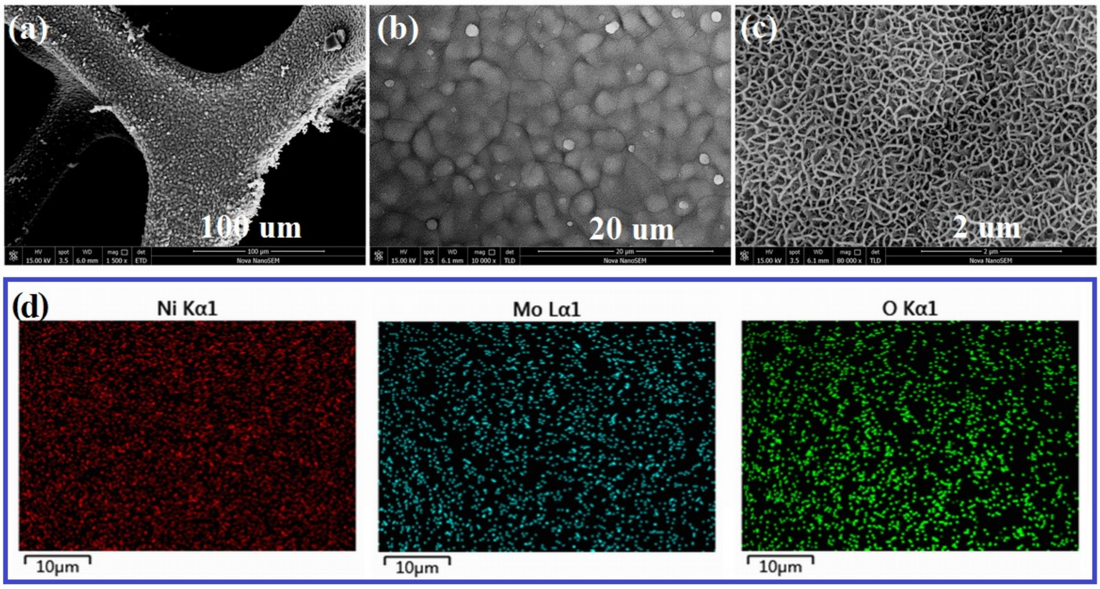


**Figure S1.** (a-c) SEM images and (d) Elements mapping of Ni2Mo1-urea0M

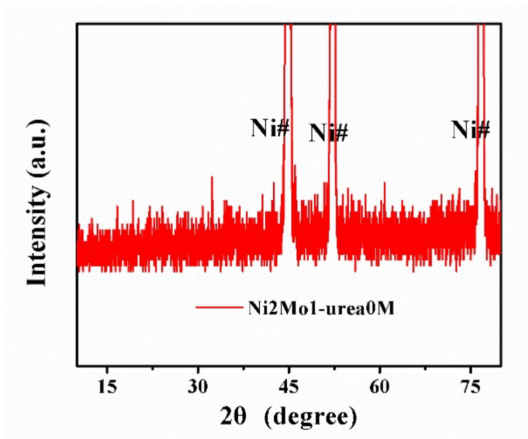


**Figure S2** XRD pattern of the Ni2Mo1-urea0M on Ni foam.

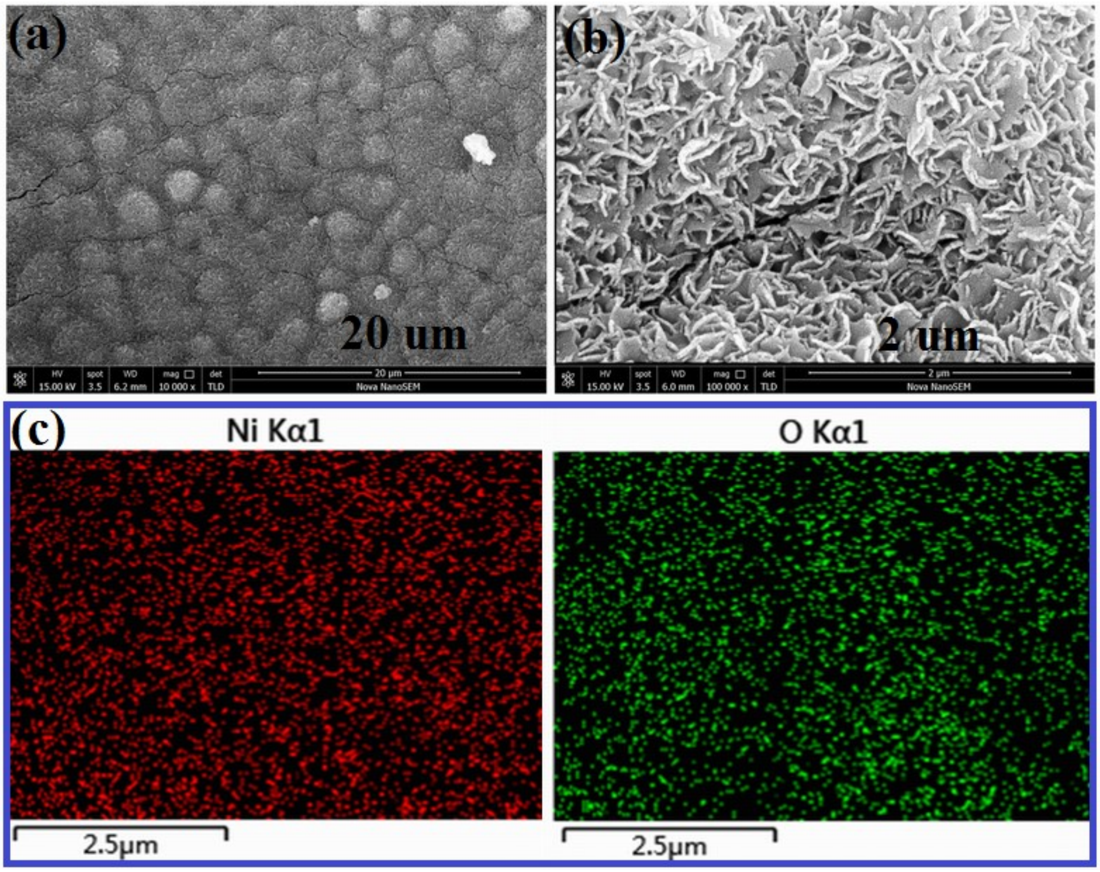


**Figure S3.** (a,b) SEM images and (c) Elements mapping of Ni2Mo0-urea0.2M

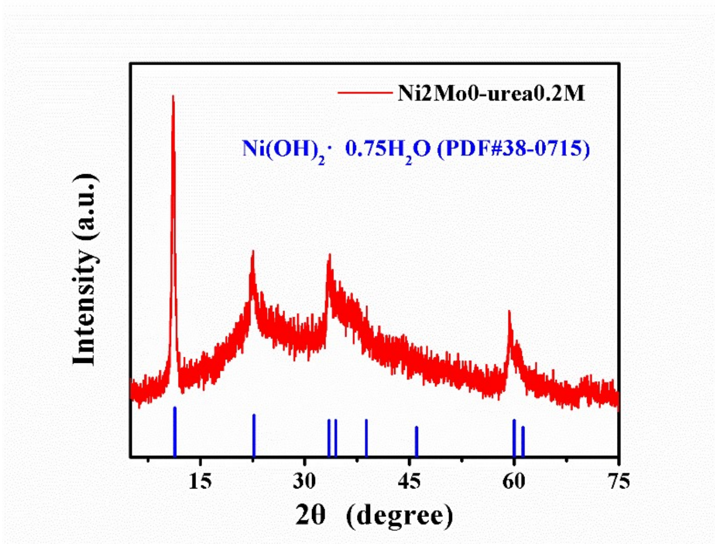


**Figure S4 XRD pattern of the Ni2Mo0-urea0.2M sample.**

In order to reduce the influence of high-strength Ni peak, we scraped the sample powder from Ni foam with a knife to test XRD. The XRD patterns of the composite (Ni2M1- urea0.2M) is drawn at **Fig.S5**. The sample shows five obvious characteristic peaks at 23.4°, 25.5°, 26.7°, 40.4°， and 52.3° which can be corresponding to the (0 2-1), (2 0 1), (2 2 0), (3 3 0), and(2 0 -4) planes of the $NiMoO_4$ (JCPDS NO. 45-0142). The peaks at 34.4°, and 60.2°correspond to the (0 1 2), and (1 1 0) planes of the $Ni(OH)_2{\cdot}0.75H_2O$ (JCPDS No. 38-0715).

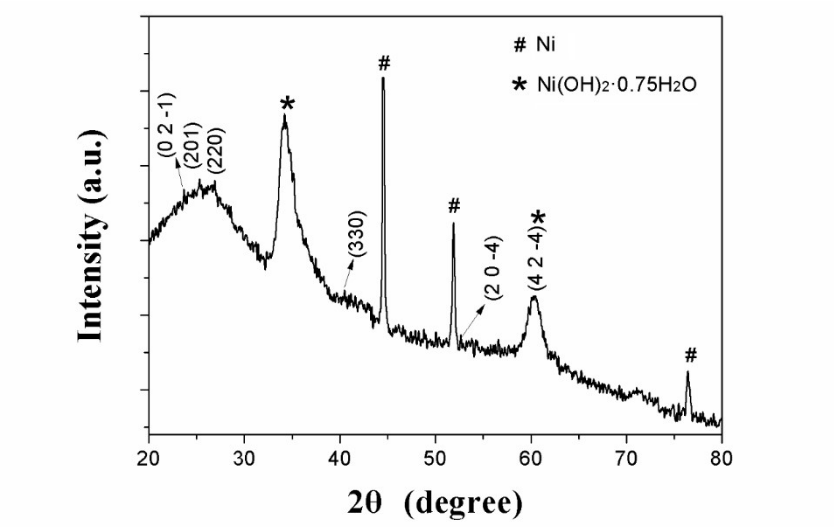


**Figure S5** the XRD patterns of the composite (Ni2Mo1- urea0.2M).

CV and GCD curves of the composite with extended urea treatment time (14h and 22h) are shown in **Fig.S6**. The different reaction time has a certain influence on the capacitance performance of the electrode. Insufficient reaction time may lead to incomplete growth of nanosheets, while too long reaction time may lead to oversized nanosheets, and the mutual coverage of nanosheets leads to a decrease in the specific surface area of the electrode, thus showing lower performance.

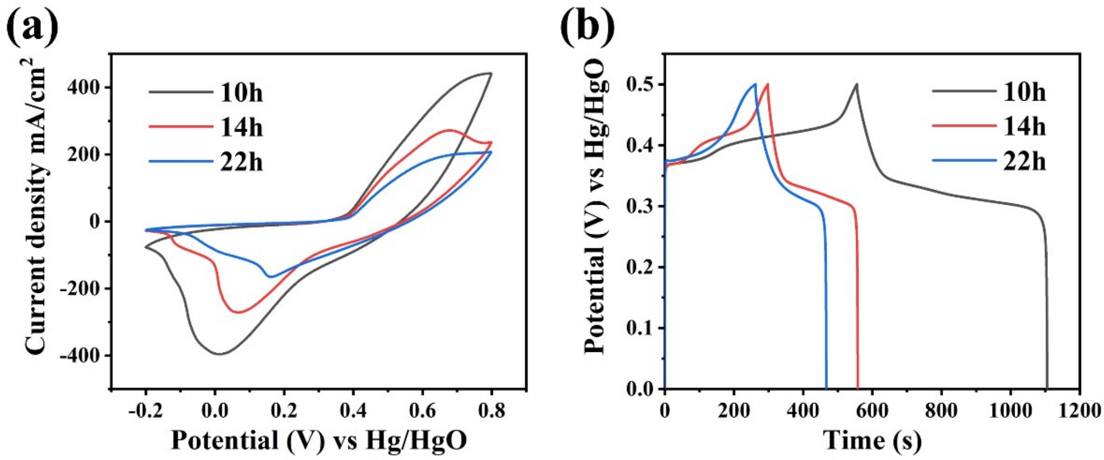


**Figure S6.** (a) CV and (b) GCD curves of the composite with extended urea treatment time (10, 14 and 22h)

**Table S1.** Area-specific capacitance of the composite with extended urea treatment time

| Sample | Discharge time of GCD (s) | Area-specific capacitance at 4 mA $cm^{-2}$ (F $cm^{-2}$) |
|---|---|---|
| 10 h | 550.3 | 4.4 |
| 14h | 259.9 | 2.1 |
| 22h | 204.8 | 1.6 |

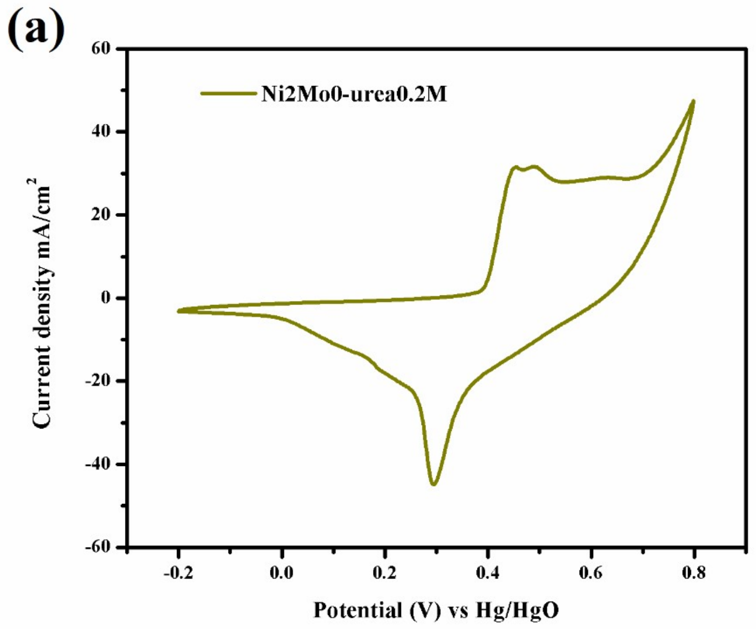


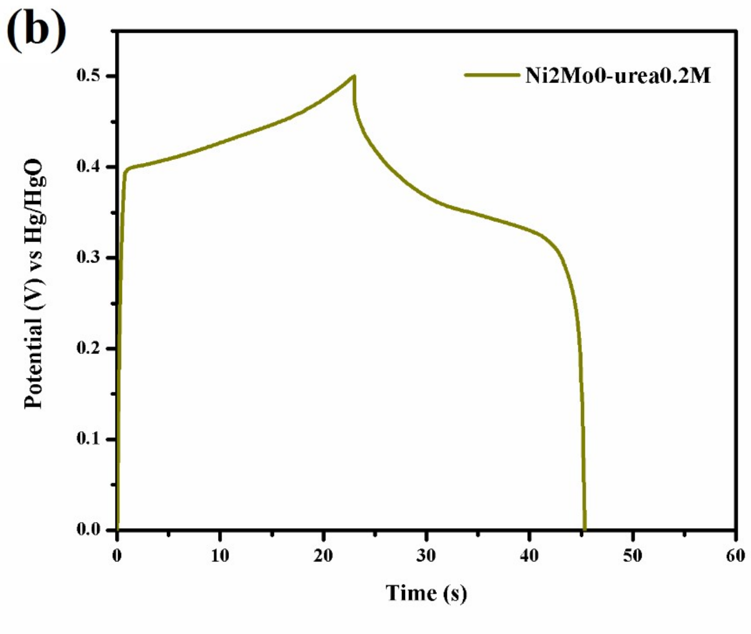


**Figure S7.** Ni2Mo0-urea0.2M electrode: (a) CV curve at 100 mV $s^{-1}$, (b) GCD curve at 4 mA $cm^{-2}$.

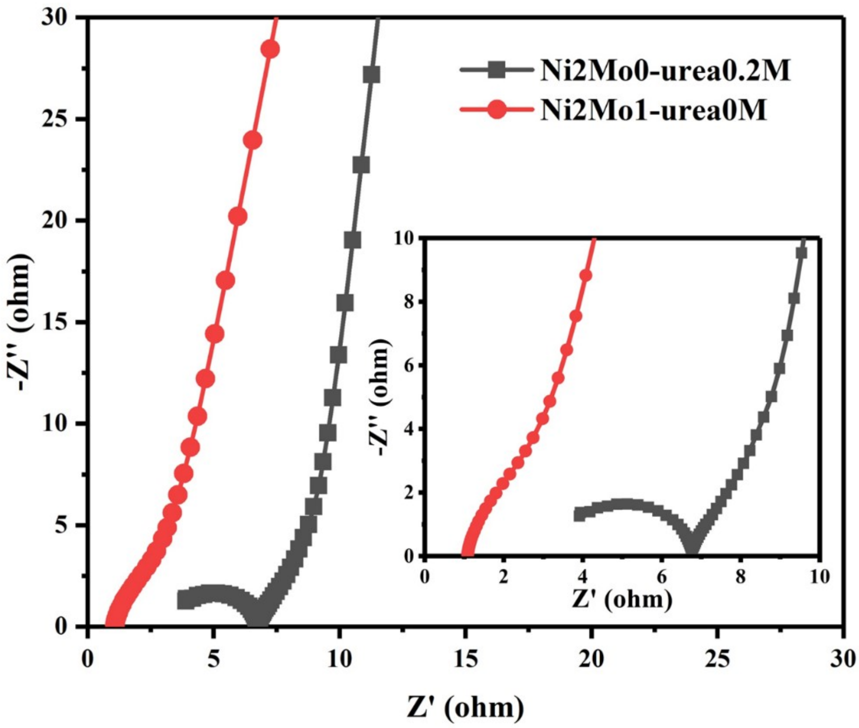


**Figure S8.** EIS of the Ni2Mo0-urea0.2M and Ni2Mo1-urea0M samples. The Rct values of Ni2Mo1-urea0M is 1.13 Ω, much smaller than Ni2Mo0-urea0.2M of 3.24 Ω, suggesting that the addition of Mo effectively improves the charge transfer performance of the active material.

The deconvoluted capacitive and insertion specific capacitance values for samples with different Mo amount are listed in **Fig.S9**. The different process contributions to the current response are analyzed using the procedure reported previously by Dunn, [S2] and Penner et al. [S3]. The capacitive capacitance and insertion capacitance of the samples shows Mo content dependent characteristics as shown in **Fig.S9**. In the deconvolution results, the capacitance increases almost linearly with the weight percentage of Mo, suggesting that the addition of Mo improves the electrical conductivity of the composite. As we know, the composite samples with higher electrical conductivity will achieve better utilization of the active materials and obtain higher capacitive capacitance. However, for Ni2Mo1-urea 0.045M sample (21.5 w.t % of Mo), it is difficult to improve the pseudocapacitance of the electrodes due to the lack of sufficient $Ni(OH)_2$ nansheets involved in Faraday reaction.

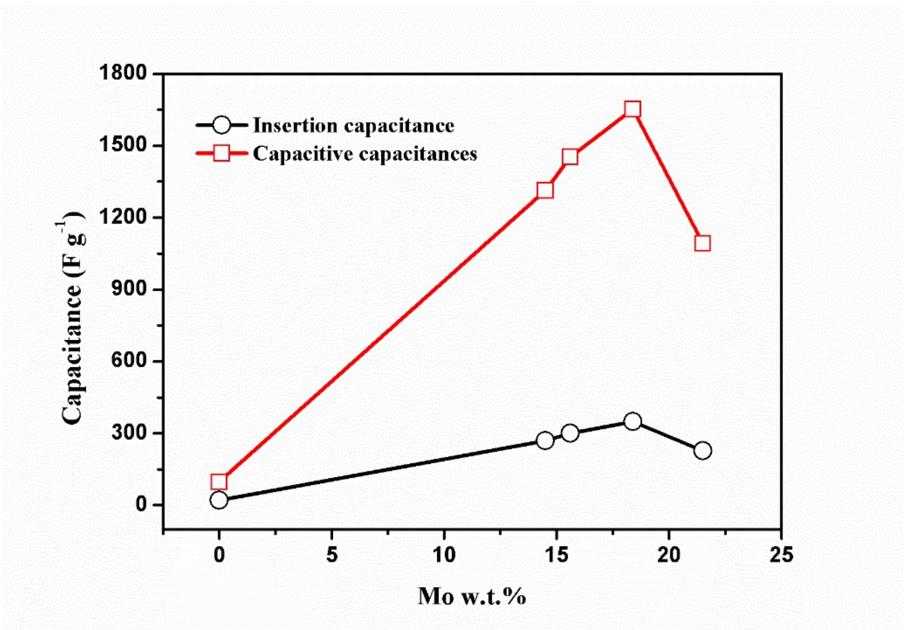


**Figure S9**. Deconvolution result of the capacitive capacitances, and insertion capacitance for composite with different w.t. % of Mo.

**Table S2.** Mass loading, area-specific capacitance and mass specific capacitance of the samples

| Sample | Mass loading ($mg\ cm^{-2}$) | Area-specific capacitance at 4 mA $cm^{-2}$ ($F\ cm^{-2}$) | Mass specific capacitance ($F\ g^{-1}$) |
|---|---|---|---|
| Ni1Mo1-urea0.36M | 1.9 | 2.0 | 1052 |
| Ni1Mo2-urea0.36M | 2.0 | 1.4 | 700 |
| Ni2Mo1-urea0.36M | 2.2 | 3.9 | 1772 |
| Ni2Mo1-rea0.045M | 2.1 | 2.8 | 1333 |
| Ni2Mo1- urea 0.2M | 2.2 | 4.4 | 2001 |
| Ni2Mo1-urea0.5M | 2.2 | 3.5 | 1590 |
| Ni2Mo1-urea 0M | 1.7 | 0.62 | 364 |
| Ni2Mo0-urea0.2M | 1.5 | 0.18 | 120 |

**Table S3.** Comparison of the key parameter of some previously reported nickel-based composite materials as ASC electrode

| Material | Capacity ($F\ g^{-1}$) | Rate capability | Energy density ($Wh\ kg^{-1}$) | Power density ($W\ kg^{-1}$) | Cycling performance | Ref. |
|---|---|---|---|---|---|---|
| $Ni(OH)_2·0.75H_2O/NiMoO_4$ (Ni2Mo1-urea0.2M) | 2001 at 1.8 A $g^{-1}$ | 63% at 21.8 A $g^{-1}$ | 70.76, 26.24 | 318.84, 7680 | 82%, 5000 cycles | This work |
| $Ni(OH)_2/MnMoO_4$ | 2658 at 1 A $g^{-1}$ | 60.5% at 10 A $g^{-1}$ | 61.4 | 428.4 | 96.4%, 7000 cycles | S4 |
| $NiMoO_4/MoS_2$ | 2003.8 at 1 A $g^{-1}$ | 72.1%, at 20 A g-1 | 49.5 | 399.8 | 81.2%, 3000 cycles | S5 |
| $MnMoO_4/MnCO_3$ | 1311 at 1 A $g^{-1}$ | 30.5% at 10 A $g^{-1}$ | 26.5 | 657.2 | 70%, 5000 cycles | S6 |
| $Ni(OH)_2/NiS$ | 1443 at 1 A $g^{-1}$ | 79.7% at 10 A g-1 | 86.2 | 800 | 87.9%, 4000 cycles | S7 |

| | | | | | | |
|---|---|---|---|---|---|---|
| $ZnCo_2O_4/Ni(OH)_2$ | 1021 at 0.3 A $g^{-1}$ | 79.7% at 3.3 A $g^{-1}$ | 40 | 802.7 | 91.2%, 5000 cycles | S8 |
| $MnS/Ni(OH)_2$ | 2612 at 1 A $g^{-1}$ | / | 60 | 800 | 86%, 1000 cycles | S9 |
| $CoMn_2O_4/Ni(OH)_2$ | 3017.9 at 0.4 A $g^{-1}$ | 74.1% at 3.2 A $g^{-1}$ | 76.2 | 1350 | 85.7%, 8000 cycles | S10 |
| $Co_3O_4/Ni(OH)_2$ | 1306.3 at 1.2 A $g^{-1}$ | 45.9% at 12.1 A $g^{-1}$ | 40 | 346.9 | 90.5%, 5000 cycles | S11 |
| $MnCo_2O_{4.5}/ Ni(OH)_2$ | 2544 at 3 A $g^{-1}$ | 82.8% at 20 A $g^{-1}$ | 56.53 | 1900 | 90.4%, 3000 cycles | S12 |
| $Ni(OH)_2/Ni(PO_3)_2$ | 1477 at 1 A $g^{-1}$ | 48.4% at 20 A $g^{-1}$ | 67 | 775 | 81%, 8000 cycles | S13 |

[S1] B. Wei, F. Ming, H. Liang, Z. Qi, W. Hu, Z. Wang, All nitride asymmetric supercapacitors of niobium titanium nitride-vanadium nitride, J. Power Sources, 481 (2021) 228842.

[S2]J. Wang, J. Polleux, J. Lim, and B. Dunn, Pseudocapacitive contributions to electrochemical energy storage in $TiO_2$ (anatase) nanoparticles. J. Phys. Chem. C 111(2007) 14925-14931.

[S3]W. Yan, T. Ayvazian, J. Kim, Y. Liu, K. C. Donavan, W. Xing, Y. Yang, J. C. Hemminger, and R. M. Penner, Mesoporous manganese oxide nanowires for high-capacity, high-rate, hybrid electrical energy storage, ACS Nano, 5(2011) 8275-8287.

[S4] H.S.Li, H.C.Xuan, Hierarchical design of $Ni(OH)_2/MnMoO_4$ composite on reduced graphene oxide/Ni foam for high-performances battery-supercapacitors hybrid device, International Journal of Hydrogen Energy,46 (2021) 38198-38211.

[S5] Q. Zong, H.Yang, Q.Q Wang, Q.L. Zhang, Y.L.Zhu, H.Y.Wang, Q.H. Shen, Three-dimensional coral-like NiCoP@C@Ni(OH)2 core-shell nanoarrays as battery-type electrodes to enhance cycle stability and energy density for hybrid supercapacitors, Chemical Engineering Journal 361 (2019) 1-11.

[S6] M.R. Pallavolu，A.N. Banerjee，R.R. Nallapureddy，W.J. Sang, Urea-assisted hydrothermal synthesis of MnMoO4/MnCO3 hybrid electrochemical electrode and fabrication of high-performance asymmetric supercapacitor, Journal of Materials Science & Technology, 96 (2022) 332-344.

[S7] K. Song, W.T. L, R.Yang, Y.J. Zheng, X.S. Chen, X.Wang,G.L. Chen, W.C. Lv, Controlled preparation of $Ni(OH)_2/NiS$ nanosheet heterostructure as hybrid supercapacitor electrodes for high electrochemical performance, Electrochimica Acta 388 (2021) 138663.

[S8] X. Han, Y. Yang, J.J. Zhou, Q. Ma, K. Tao, L. Han, Metal-organic framework templated 3D hierarchical $ZnCo_2O_4@Ni(OH)_2$ core-shell nanosheet arrays for high-performance supercapacitors, Chemistry-A European Journal, 24 (68) (2018) 18106-18114.

[S9] P. Naveenkumar, M.Maniyazagan, J. Yesuraj, H.W. Yang, N. Kang,, K.Kim, G. P. Kalaignan, W.S. Kang, S.J. Kim, Electrodeposited $MnS@Ni(OH)_2$ core-shell hybrids as an efficient electrode materials for symmetric supercapacitor applications, Electrochimica Acta, 412 (2022) 140138.

[S10] W.G. Huang, J. Lia,, S.H. Wang, S.D. Tao, Y.H. Xiao, Y.Y. Zhang, L.H. Wang, J. Luo, Highly-active $CoMn_2O_4$ nanowires decorated with multilayer $Ni(OH)_2$ nanosheets as bind-free electrodes for high-performance energy storage application, Journal of Alloys and Compounds 909 (2022) 164551.

[S11] X.Bai, Q.Liu, J.Y. Liu, H.S. Zhang, Z.S. Li, X.Y. Jing, P.L. Liu,J.Wang, R.M. Li, Hierarchical $Co_3O_4@Ni(OH)_2$ core-shell nanosheet arrays for isolated allsolid state supercapacitor electrodes with superior electrochemical performance, Chemical Engineering Journal, 315 (2017) 35-45.

[S12] Y.L. Liu, C. Yan, G.G. Wang, H.Y. Zhang, L.Y. Dang, B.W. Wu, Z.Q.Lin, X.S. An, J.C.Han, Achieving ultrahigh capacity with self-assembled $Ni(OH)_2$ nanosheet decorated hierarchical flower-like $MnCo_2O_{4.5}$ nanoneedle as advanced electrode of battery-supercapacitor hybrid device, ACS Applied Materials & Interfaces 11 (2019)

9984-9993.

[S13] J.Y. Hao, X.F. Zou, L. Feng, W.P. Li, B.Xiang, Q. Hu, X.Y. Liang, Q.B. Wu, Facile fabrication of core-shell structured $Ni(OH)_2/Ni(PO_3)_2$ composite via one-step electrodeposition for high performance asymmetric supercapacitor, Journal of Colloid and Interface Science 583 (2021) 243-254.